Orbit Design for Phase I and II of the Magnetospheric Multiscale Mission

Steven P. Hughes*

The Magnetospheric Multiscale Mission (MMS) is a NASA mission intended to make fundamental advancements in our understanding of the Earth's magnetosphere. There are three processes that MMS is intended to study including magnetic reconnection, charged particle acceleration, and turbulence. There are four phases of the MMS mission and each phase is designed to study a particular region of the Earth's magnetosphere. The mission is composed of a formation of four spacecraft that are nominally in a regular tetrahedron formation. In this work, we present optimal orbit designs for Phase I and II. This entails designing reference orbits such that the spacecraft dwell-time in the region of interest is a maximum. This is non-trivial because the Earth's magnetosphere is dynamic and its shape and position are not constant in inertial space. Optimal orbit design for MMS also entails designing the formation so that the relative motion of the four spacecraft yields the greatest science return. We develop performance metrics that are directly related to the science return, and use Sequential Quadratic Programming (SQP) to determine optimal relative motion solutions. While designing for optimal science return, we also consider practical constraints such as maximum eclipse time and minimum inter-spacecraft separation distances. Data are presented that illustrates how long we can ensure that the formation remains in the relevant region of the Earth's magnetosphere. We also draw general conclusions about where in the orbit acceptable tetrahedron configurations can be provided and for how long.

INTRODUCTION

The MMS mission is one of several missions in NASA's Solar Terrestrial Probes (STP) program. The goal of MMS is to make fundamental advancements in our understanding of the Earth's magnetosphere and its dynamic interaction with the solar wind. Much of the previous research has been limited due to the reliance on single-spacecraft measurements which are not adequate to reveal the underlying physics of highly dynamic, highly structured plasma processes. By taking advantage of the latest multi-spacecraft mission technology, MMS will be able to differentiate between spatial and temporal effects to determine the three-dimensional geometry of the plasma, field, and current structures under study.[1]

MMS is not the first mission to use multiple spacecraft to study magnetospheric dynamics. The Cluster II mission was successfully launched by the European Space Agency (ESA) in the summer of 2000 and has already provided fascinating results on magnetospheric dynamics. The primary difference between MMS and Cluster II is the relative distances of the spacecraft in formation. The relative distances of the MMS spacecraft are expected to be several orders of magnitude smaller than the distances of the Cluster II spacecraft. A detailed comparison of MMS and Cluster II is beyond the scope of this paper. However, due to the large difference in formation dimensions, the science return for MMS and Cluster II are likely to complement each other well.

*Aerospace Engineer, Flight Dynamics Analysis Branch, NASA Goddard Space Flight Center, (301) 286-0145, (301) 286-0369 (FAX), email: Steven.P.Hughes@nasa.gov

There have been many important contributions to the literature for orbit design for magnetospheric missions. Stern[6,7] presented a systematic approach for designing orbits for magnetospheric missions. In Ref. [6], Stern assumed an equatorial mission orbit to maximize mass to orbit. However, for the work presented here we will not limit the design to equatorial orbits. In Ref. [7], Stern builds upon his previous results and presents a mission known as Profile. In Profile a "String of Pearls" orientation of multiple spacecraft are used to investigate magnetospheric processes near the Earth's equator. Hughes[2] developed an approach to provide optimal tetrahedron geometries for Phase I of MMS, and quantified the achievable performance with natural Keplerian motion.

To provide the best possible orbit design for the MMS mission, we must take the science objectives described above, and develop a numerical relationship between the orbit evolution and the science data return. We need to ensure the formation of spacecraft passes through the desired region of the magnetosphere, taking into account the non-linear evolution of the orbits due to perturbations, and the non-linear dynamics of the magnetosphere itself. We also need to ensure that the relative motion of the spacecraft in formation provides optimal science return.

According to the latest documentation,[1] the region of the magnetosphere of primary interest is the plasma sheet region. We discuss this region and its dynamics in more detail in a later section. However, with the region of interest of the magnetosphere well-defined, we can define one goal for the orbit design: *We wish to maximize the total time the formation spends in the plasma sheet region of the magnetosphere.* This problem is complicated by practical constraints such as maximum eclipse time which will be discussed in a later section.

We know the optimal relative geometry of the four spacecraft is a regular tetrahedron. However, it is not possible to provide a regular tetrahedron for an entire orbit using only Keplerian motion. Furthermore, due to fuel constraints and operational limitations of spinning spacecraft, continuous feedback control of the formation to maintain a regular tetrahedron is probably not feasible. Hence in this work, we investigate the tetrahedron quality that can be provided by four spacecraft using Keplerian motion only. The tetrahedron quality is a function that depends on the size of the tetrahedron and its shape. Hence we can state a second goal: *We wish to maximize the tetrahedron quality when the formation is in scientifically interesting regions of the magnetosphere.*

As stated above, we assume that the science return is dependent on both the reference orbit design, and the relative motion of the spacecraft in formation. However, due to the nature of the science, and the fact that the relative separations of the spacecraft are small in relation to the orbit dimensions, we assume that we can solve for the reference orbit and relative motion solutions independently, without loss of generality. This allows for some significant simplification of the problem. However there are still considerable difficulties to address. In the next section we present in detail the methods used to determine optimal reference orbits and relative motion solutions.

ORBIT DESIGN

Designing optimal spacecraft orbits for MMS necessitates that we find orbits that spend the maximum amount of time in the magnetosphere while simultaneously providing a maximum tetrahedron quality factor during regions of interest. We assume that providing such a set of orbits maximizes science return. Due primarily to the fact that the tetrahedron dimensions are several orders of magnitude less than the dimensions of the reference orbit, we assume we can decouple the relative motion from the reference motion and solve for the optimal solutions for these problems separately.

While providing optimal reference orbits and relative motion configurations we must simultaneously consider many mission constraints. The mission constraints are determined by both the science objectives and practical limitations determined by the spacecraft design. Some of the constraints

need to be taken into account when designing the reference orbit, while others only affect the tetrahedron design. For example, the maximum allowable eclipse duration is taken into account in the reference orbit design. The minimum inter-spacecraft separation distance is taken into account in the relative motion design. In some cases it is easier to use a penalty function approach to ensure a constraint is satisfied. In other cases it is more effective to express a constraint as either a linear, bound, or non-linear constraint and let an SQP algorithm ensure the constraint is satisfied. The handling of the mission constraints is discussed in detail in their appropriate sections.

While determining the mission orbits is the topic of this research, a nominal orbit configuration for Phase I and II is suggested and is shown here in Table 1. In the next subsection we use the

Table 1: Properties of MMS Orbits Phase I and II

Property	Phase I	Phase II
r_p	1.2 R_e	1.2 R_e
r_a	12.0 R_e	30.0 R_e
T	0.995 *days*	3.615 *days*
a	42096 *km*	99499 *km*
e	0.8182	0.9230
i	10.0°	10.0°
ω	90.0°	90.0°
Ω	0.0°	0.0°
Tetrahedron Size	10 *km*, 1000 *km*	10 *km*, 1000 *km*

nominal orbits as a reference solution and investigate how well similar orbits provide configurations for maximal science return for MMS. After investigating the reference orbit, we present a method for designing optimal tetrahedron formations.

Reference Orbit Design

Our primary goals in designing a reference orbit for MMS are to maximize the science return and to satisfy mission constraints. We assume that we can maximize science performance by maximizing the time the reference orbit spends in the plasma sheet region of the Earth's magnetosphere. Hence our performance metric for the reference orbit design can be written as

$$J_{ref} = \sum_i \Delta t_i \tag{1}$$

where Δt_i is the dwell time of the i^{th} passage of the reference spacecraft through the plasma sheet region. By summing over i we obtain the total time the reference spacecraft spends in the plasma sheet region.

To evaluate Eq. (1) we need a model of the plasma sheet region and its dynamic motion in time. A diagram that illustrates the different regions of the magnetosphere, including the plasma sheet region, is found in Figure 1. The magnetosphere moves nonlinearly with respect to inertial space. One cause of this motion is that the Earth's magnetic dipole is not in line with the Earth's spin axis. This causes the magnetosphere to rock in inertial space with a period of one day. Another cause for the nonlinear motion of the Earth's magnetosphere is that the orientation of the Earth's magnetic pole with respect to the incoming solar wind changes over the course of the year. During the summer season in the northern hemisphere, the dipole is tilted toward the sun. During the winter season in the northern hemisphere, the dipole is tilted away from the sun. A final cause for the motion of the magnetosphere is the dynamic nature of the incoming solar wind. For this work

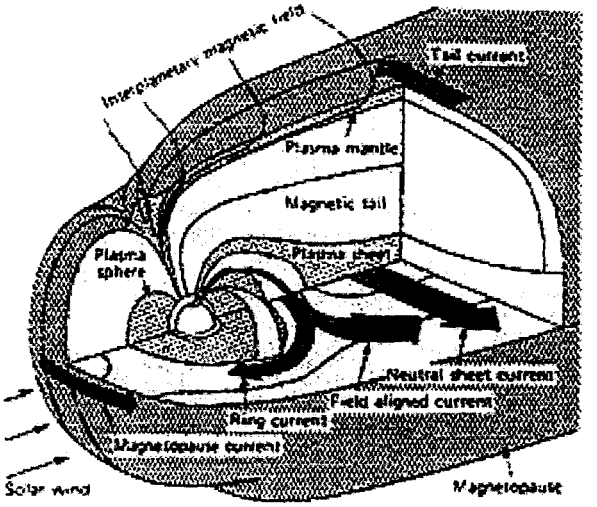

Figure 1: The Earth's Magnetosphere

we use a model of the Magnetosphere developed by Tsyganenko[8-12] and we refer the reader to the references for further details on the model.

For the reference orbit optimization the problem is greatly simplified if we choose to parameterize the problem using Keplerian orbital elements. The orbit dimensions, r_p and r_a, for Phase I and II are given in Table 1. These dimensions ensure the orbit does not extend too far from the Earth such that orbit apogee is beyond the interesting region of the plasma sheet. Given r_p and r_a, we can determine the semimajor axis and eccentricity of the reference orbits for Phase I and II. However, the inclination, i, the argument of periapsis, ω, the right ascension of the ascending node, Ω, and the true anomaly at the initial epoch ν_i, are still undefined. Hence we can write

$$J_{ref} = f(i, \omega, \Omega, \nu_i) \tag{2}$$

In reality, J_{ref} is an explicit function of the initial epoch because the perturbations of the Sun and Moon are explicit functions of time . However, the current launch date for MMS is early 2010 and we have assumed an initial epoch of March 22, 2010 at 12:00:00:0000 UTC.

There are several important constraints to consider in the reference orbit design. We consider constraints on the maximum eclipse duration and the minimum allowable periapsis. The maximum allowable eclipse duration is determined by the spacecraft power system capabilities. The minimum allowable periapsis is determined primarily by reentry concerns, but also is dependent on the science goals. We have chosen to perform parametric scans over a range of the independent variables to establish the relationship between the independent variables and the cost and constraints. The motivation for doing so is to provide data which can allow us to draw some general conclusions about the design space and its properties. We desire to find solutions that maximize the dwell time in the Plasma Sheet. However, we also need to ensure we do not violate the maximum eclipse constraint or the minimum periapsis constraint. Due to the fact that these constraints have not been well defined at this time, we cannot solve for individual solutions to the optimal reference orbit problem. However, having a good understanding of the relationship between the independent variables and the cost and constraints is invaluable. We can provide this understanding by performing appropriate parametric scans and presenting the data in a useful way.

To perform parametric scans we have chosen to vary the independent variables in increments of 2°, with upper and lower bounds defined by

$$10^o < \quad i \quad < 28^o \tag{3}$$
$$80^o < \quad \omega \quad < 100^o \tag{4}$$
$$-10^o < \quad \Omega \quad < 10^o \tag{5}$$
$$\tag{6}$$

The initial true anomaly, ν_i, is held constant at zero for reasons explained in a later section. For each set of initial conditions we propagate the reference orbit for 6 months. For the 6 month propagation we determine the dwell time in the plasma sheet, the maximum eclipse duration, and the minimum radius of periapsis for each solution. The force model is a 4x4 non-spherical gravity field (JGM-2), with perturbations from the Sun and Moon (DE200). The performance and constraint data is included in a later section.

In summary, for the reference orbit design, we wish to maximize the dwell time of the formation of spacecraft in the plasma sheet region of the magnetosphere. We assume that the formation dimensions are small enough that we can solve the reference orbit optimization problem by only considering the dwell time of the reference spacecraft. We perform a set of parametric scans in order to determine the relationship between the independent variables and the dwell time of the reference spacecraft. The relationship between the independent variables and the constraints are also presented. The results for the reference orbit design are presented in a later section. Before discussing the results we present the design approach for finding optimal relative motion solutions.

Relative Motion Design

The science return from the four MMS spacecraft is intimately dependent on the relative motion of the spacecraft in formation. To maximize science return it is desirable for the spacecraft to maintain a regular tetrahedron over the entire orbit. However this is not possible using Keplerian orbits and using active control to maintain a regular tetrahedron is prohibitively costly. Hence we wish to find the relative motion that provides the maximum performance possible with Keplerian orbit dynamics. Our goal is to characterize the performance that we can provide by carefully optimizing the relative motion of the four spacecraft. In general the performance will vary in time and it is important to determine for which regions of the reference orbit we can provide acceptable science return. In this subsection we present an approach to determine optimal relative motion solutions. The method was developed previously by Hughes,[2] and we refer the reader to the reference for a more detailed discussion.

We begin by developing a metric that allows us to ascertain the science return provided by a particular relative geometry at a given instant. Then, given the instantaneous performance metric, we develop another metric that allows us to determine the performance of a particular orbit design over a specific region of interest in the orbit. There are many different possible formulations for an instantaneous tetrahedron quality metric, and we have chosen one based on work by Glassmeier.[3] Glassmeier's metric is written as

$$Q_{GM} = \frac{V_a}{V^*} + \frac{S_a}{S^*} + 1 \tag{7}$$

where V_a is the actual volume of a given tetrahedron, S_a is the actual surface area of a given tetrahedron, V^* is the volume of a regular tetrahedron with sides equal to the average side length of the actual tetrahedron, and S^* is the area of a regular tetrahedron with sides equal to the average side length of the actual tetrahedron. It is important to note that the following two relations are always true:

$$V_a \leq V^* \tag{8}$$

$$S_a \leq S^* \tag{9}$$

Hence, the maximum value of Q_{GM} is three and this occurs when the formation is in a regular tetrahedron configuration. The value of Q_{GM} is one when the formation is collinear, or collocated. Glassmeier's quality metric provides a way of determining the regularity of a tetrahedron. However, it is important to note that it does not give any information about the size of the tetrahedron. All regular tetrahedrons, regardless of the side length L, have the property $Q_{GM} = 3$. This is a concern because the size of the tetrahedron formation is important for MMS.

We propose a modification to Glassmeier's metric to allow it to contain information on not only the tetrahedron shape, but also its size. There are many ways in which we can modify Q_{GM} to include information on the tetrahedron's size. Before we modify Q_{GM}, we define a simple function $S(L^*)$ as follows:

$$S(L^*) = \begin{cases} 0 & L^* < \ell_l \\ (L^* - \ell_1)^2(L^* + \ell_1 - 2\ell_2)^2/(\ell_2 - \ell_1)^4 & \ell_l < L^* < \ell_2 \\ 1 & \ell_2 < L^* < \ell_3 \\ (L^* - \ell_4)^2(L^* - 2\ell_3 + \ell_4)^2/(\ell_4 - \ell_3)^4 & \ell_3 < L^* < \ell_4 \\ 0 & L^* > \ell_4 \end{cases} \tag{10}$$

where L^* is the average side length, and ℓ_1, ℓ_2, ℓ_3, and ℓ_4 are chosen according to the desired dimensions of the tetrahedron. In Table 2, the values of ℓ_1, ℓ_2, ℓ_3, and ℓ_4 used in this work for the 10 km and 1000 km tetrahedron are shown. A graph of $S(L^*)$ for the 10 km tetrahedron is shown in Figure (2) and provides an intuitive description of the function. For the 10 km tetrahedron we have designed $S(L^*)$ to be zero when the average side length is not near 10 km. The limits are chosen so that $S(L^*)$ is zero for tetrahedrons with average side lengths of less than 2 km, or greater than 20 km.

Table 2: Values of ℓ_i for 10 km and 1000 km tetrahedrons

Tetrahedron Dimension	ℓ_1	ℓ_2	ℓ_3	ℓ_4
10 km	2	4	18	20
1000 km	700	800	1200	1300

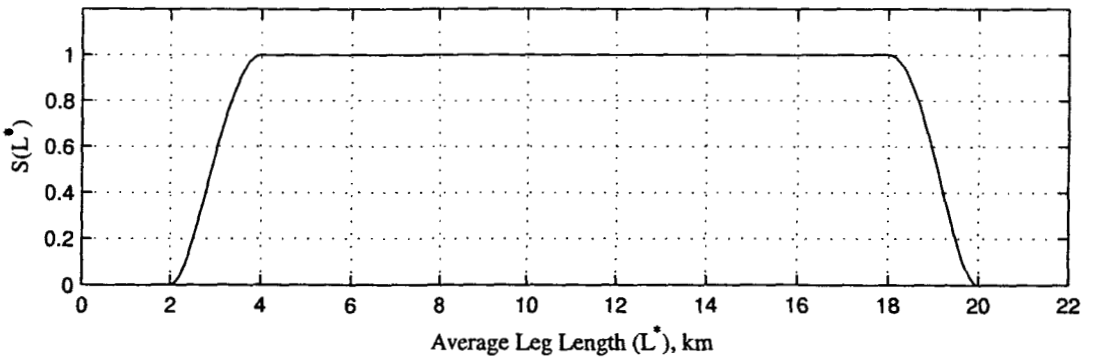

Figure 2: Plot of $S(L^*)$

By posing a composite quality metric Q_C defined as

$$Q_C = Q_{GM} * S(L^*) \tag{11}$$

we have a metric that contains information on both the size and shape of the tetrahedron. When the value of Q_C is three, we know that the formation is in a regular tetrahedron configuration, and that the side length is somewhere between 4 and 18 km.

Given an instantaneous measure of performance, we need to formulate a general expression to provide a measure of performance over a region of interest along the reference orbit. After considering several forms we have chosen a form shown in Eq. 12

$$J(\mathbf{X}) = \frac{1}{\nu_f - \nu_i} \int_{\nu_i}^{\nu_f} (3 - Q_{GM} S(L^*)) \; d\nu \tag{12}$$

where ν_i is the initial true anomaly defining the beginning of the region of interest, and ν_f is the final true anomaly and defines the end of the region of interest. This metric is proportional to the area between the ideal performance and actual performance curves, because according to Eq. (11) the ideal instantaneous performance is always three. When the integral in Eq. (12) is zero, the performance is ideal over the entire region of interest. The choice of independent variables, $\mathbf{X}$, is important in the success of an optimization process and can affect the final solution and the time to converge for an iterative method. There are many possibilities for choosing independent variables for performance metric shown in Eq. (12). However, if we choose to work in Keplerian elements, the problem is greatly simplified.

While solving for optimal relative motion solutions we assume Keplerian motion, so the orbit dynamics are not explicit functions of time. Therefore, there are six state variables associated with the orbit state of each of the four spacecraft. Hence, there is a maximum of 24 independent variables for describing the motion. However, we require that the periods of all the orbits must be equal. This is equivalent to the following three constraints

$$\begin{aligned} a_1 &= a_2 \\ a_2 &= a_3 \\ a_3 &= a_4 \end{aligned}$$

where a_1 is the semimajor axis of orbit one and so on. If we choose to work in Keplerian elements these constraints can be satisfied implicitly. The vector of independent variables chosen for this work is

$$\mathbf{X} = [a \; e_1 \; i_1 \; \omega_1 \; \Omega_1 \; \nu_1 \; e_2 \; i_2 \; \omega_2 \; \Omega_2 \; \nu_2 \; e_3 \; i_3 \; \omega_3 \; \Omega_3 \; \nu_3 \; e_4 \; i_4 \; \omega_4 \; \Omega_4 \; \nu_4]^T \tag{13}$$

where a is the semimajor axis of all orbits, e is the eccentricity, i is the inclination, ω is the argument of periapsis, Ω is the right ascension of the ascending node, ν is the true anomaly, and the subscripts represent the spacecraft number.

Recall that for Phase I the nominal orbit dimensions are 1.2 x 12 R_e, and for Phase II the nominal dimensions are 1.2 x 30 R_e. We must impose additional constraints on $\mathbf{X}$ to ensure that the orbit solutions have dimensions similar to the nominal orbit dimensions. In this work we have not tried to meet these constraints exactly. Rather, we wish to characterize the performance possible using orbits with dimensions near nominal orbit dimensions. There are several motivating factors for this work. First, the solutions are computationally demanding and relaxing some constraints is helpful to find solutions efficiently. Secondly, the allowable tolerances on the orbit dimensions have not been specified by the MMS Project. The bound constraints on the orbital elements are shown in Table 3.

There are numerous choices for numerical optimization routines that are applicable for this work. Because we have bound constraints on the independent variables, we must choose a method that can handle linear constraints. For this work we have chosen to use SQP. The specific package we have chosen to use is MATLAB's *fmincon* function. For details on the *fmincon* routine, we refer the

Table 3: Bound Constraints Used in Relative Motion Optimization

Property	Phase I, 10 km	Phase I, 1000 km	Phase II, 10 km
a	$41905\ km < a < 43905\ km$	$41905\ km < a < 43905\ km$	$97745\ km < a < 101253\ km$
e	$0.80 < e < 0.80$	$0.80 < e < 0.80$	$0.92125 < e < 0.92495$
i	$9.5° < i < 10.5°$	$-\infty < i < \infty$	$-\infty < i < \infty$
ω	$85.293° < e < 95.293°$	$-\infty < \omega < \infty$	$-\infty < \omega < \infty$
Ω	$-\infty < \Omega < \infty$	$-\infty < \Omega < \infty$	$-\infty < \Omega < \infty$
ν_i	$-\infty < \nu_i < \infty$	$-\infty < \nu_i < \infty$	$-\infty < \nu_i < \infty$

reader to the documentation for MATLAB's *Optimization Toolbox*.[5] There are no known analytic formulations for the gradient of the performance metric described in Eq. (12) with respect to the independent variables described in Eq. (13). Hence, for this work all of the derivatives are calculated using finite differencing. The algorithm used to develop an initial guess for the independent variables is presented in Ref[2].

To pose an optimization problem we must formulate a performance metric and choose a set of independent variables. If using an iterative approach we must also provide an initial guess. In this section we developed a performance metric that relates the relative motion of the four MMS spacecraft to the science return for the mission. We posed a set of bound constraints to ensure that the optimal solutions have the appropriate dimensions for the MMS mission. In the next section we present the results for the reference orbit and relative motion design. We discuss one solution in detail, and then present some general conclusions.

RESULTS

For multiple spacecraft missions such as MMS, the science return is intimately dependent upon the orbit design. The coupling between the science return and the orbit design is much stronger than most single spacecraft missions. The strong coupling is due to the fact that the entire formation serves as the science instrument. The relative spacing of the spacecraft in formation, and the placement of the reference orbit in inertial space, are therefore a part of designing the science instrument itself. In this section we present some design solutions that maximize the performance of the MMS formation according to metrics discussed in the previous section. We first present results for the reference orbit design. The relationships between the independent variables for the reference orbit design and the performance and constraints are discussed. Where possible we identify some general conclusions that can be made. Next we present the results of the relative motion optimization. We present the results of one optimal case in detail. Following we present some general results and discuss where along the reference orbit it is possible to provide adequate performance. Finally, we present results that illustrate how long different formations will remain in optimal configurations in the presence of natural perturbations.

Reference Orbit Results

Recall that our goal in designing optimal reference orbits for Phase I and Phase II is to maximize the time the reference spacecraft spends in the plasma sheet region of the Earth's magnetosphere. This is called the dwell time. However, we must simultaneously satisfy several mission constraints. We know that the maximum eclipse duration and the evolution of the periapsis altitude will be important drivers for selection of a reference orbit. However, firm numbers for a maximum eclipse and minimum periapsis altitude have not been clearly defined yet. As a result, we present data that demonstrates how the reference orbit performance, and the constraints are related to the independent variables.

For the reference orbit design the independent variables are the inclination, i, the argument of periapsis, ω, the right ascension of the ascending node, Ω, and the true anomaly at the initial epoch, ν_i. Figure 3 contains plots of the dwell time of the reference spacecraft in the plasma sheet for possible Phase I orbits. The x-axis and y-axis are ω and i respectively. The solid contour lines are lines of constant dwell time with units in days. The dotted contour lines illustrate lines of constant maximum eclipse duration with units in hours. For each plot, Ω is a constant and the value of Ω for the individual plots is shown. The true anomaly at the initial epoch, ν_i, is constant for all plots and is equal to zero. For Phase I, the drift in the periapsis altitude due to the lunar perturbation was minimal varying between -160 km and -230 km for all solutions. For this reason, contours of the periapsis drift are not included to keep the plots as simple as possible.

From the plots in Figure 3 is it possible to draw conclusions about the relationship between i, ω, and Ω and their influence on the dwell time and maximum eclipse duration for Phase I. Inclinations below 14° all exhibit dwell times of 46 days or greater. The argument of periapsis plays an important role. For values of ω near 80° it is possible to achieve dwell times of near 50 days, at inclinations around 21°. It is desirable to find orbits that have long dwell times at inclinations near 28.5° in order to maximize the mass-to-orbit launching from Kennedy Space Center. However, for inclinations near 28.5° the maximum eclipse durations are on the order of 3.5 hours which is prohibitively high. At an inclination of 10° it is possible to provide a dwell time of 61.5 days. However, it is not clear if such a low inclination is achievable while simultaneously providing an acceptable mass to orbit.

It is important to note that the plots shown in Figure 3 assume that the true anomaly at initial epoch, ν_i, is zero. This assumption plays an important role for the Phase I results. Recall that the plasma sheet dynamics have a short periodic term with a period of one day. Since the period of the current nominal Phase I orbit is also one day, it is possible to dramatically change the dwell time choosing a different true anomaly at initial epoch. *The coupling between the initial position within the reference orbit and the initial epoch, T_i, can result in extremely short dwell times if the values are not chosen carefully.* However, if T_i and ν_i are chosen carefully, then it is possible to provide longer dwell times at higher inclinations, than is possible for reference orbits that do not have a period equal to an integer number of days. This is illustrated by comparing the results seen in Figure 3 with the results for shown in Figure 4. The results in Figure 4 were created by raising the periapsis of the Phase I reference orbit to 2.5 R_e. For this orbit the period is approximately 1.15 days. As seen in Figure 4, at high inclinations the dwell times are much lower, for the same values of i, Ω, and ω, than solutions in Figure 3. This is in part due to the fact that the period of the orbit is not an integer multiple of days. The dwell times are also lower because the reference spacecraft moves faster while in the plasma sheet region for the reference orbit with $r_p = 2.5\ R_e$. Hence the trade between choosing a reference orbit with a period of near 1 day is that we can provide longer dwell times, but we have the operational concern of acquiring and maintaining a specific true anomaly at the appropriate epoch.

Examining the contour lines of constant maximum eclipse in Figure 3, we see that the inclination has the strongest influence on the eclipse duration for Phase I. The maximum eclipse time is only weakly influenced by ω and Ω with exceptions for inclinations less than 16°. The largest maximum eclipse durations occur near inclinations of 23.5°. This occurs because an inclination of 23.5° places the orbit apogee near the ecliptic plane. Hence the spacecraft is moving relatively slowly when it passes through the Earth's shadow. For orbits near the ecliptic plane we see maximum eclipse durations of around 3.9 hours for Phase I. In general, to ensure the maximum eclipse duration does not exceed 2 hours during Phase I, we must use inclinations of 15° or less.

In Figure 5 we see contour plots of the dwell time and maximum eclipse duration for possible Phase II reference orbits. For the plots ν_i was assumed to be zero. However, since the orbit period for Phase II is not an integer number of days, the plots do not change significantly for different values

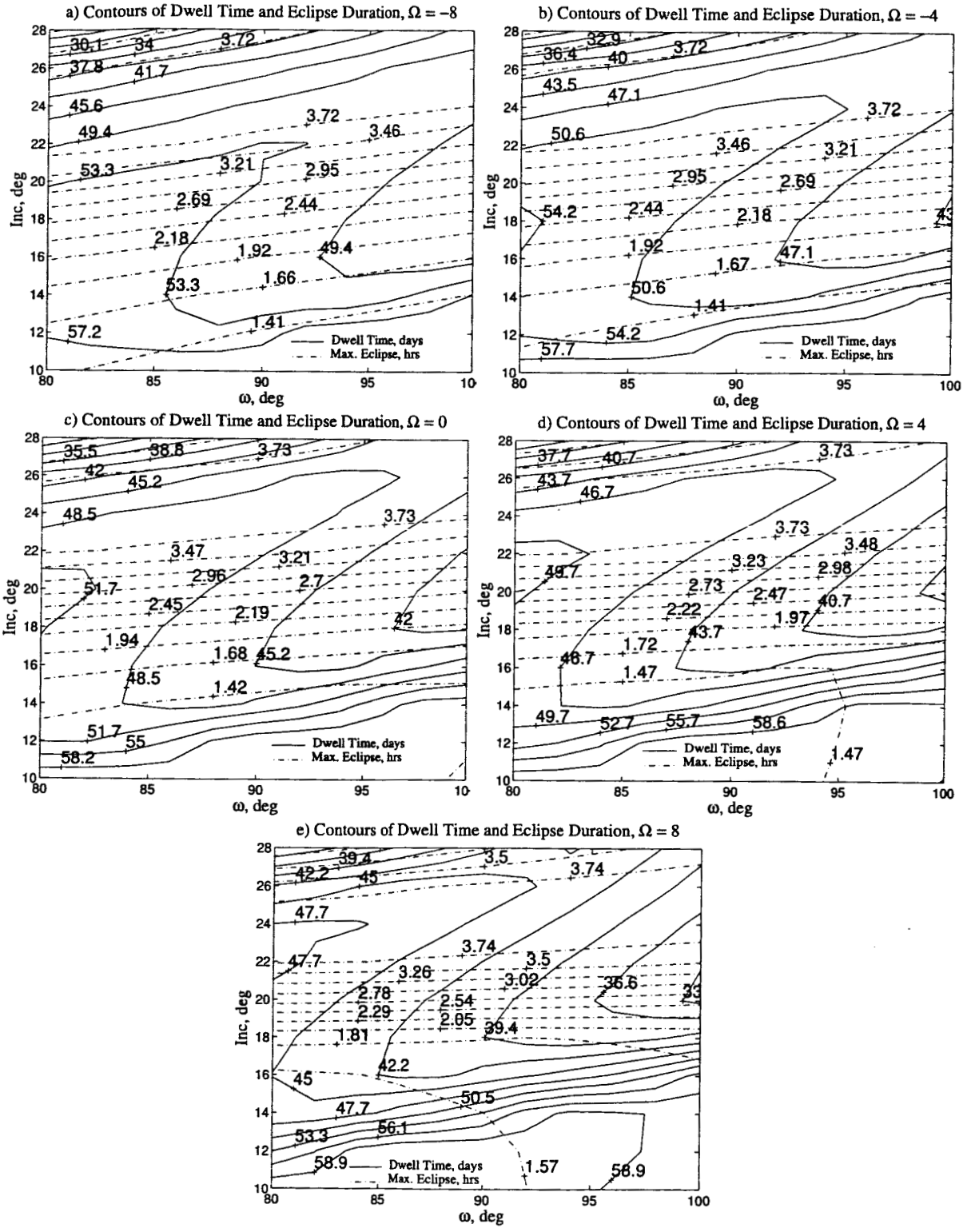

Figure 3: Contours of Dwell Time and Maximum Eclipse Duration for Phase I

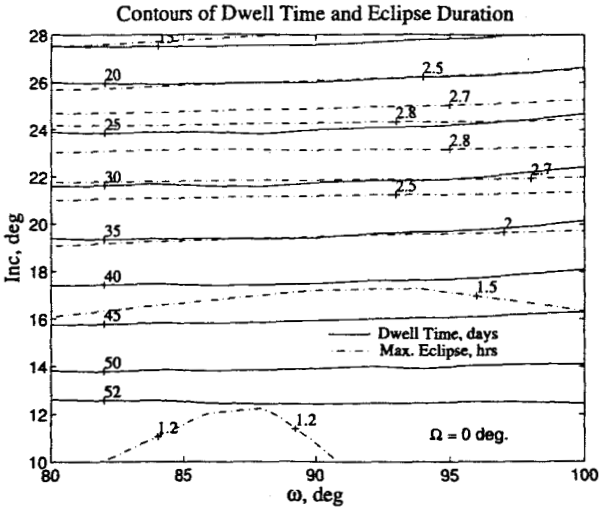

Figure 4: Contours of Dwell Time and Maximum Eclipse Duration for Phase I, $r_p = 2.5R_e$

of ν_i. It is important to note that for these plots, the initial radius of periapsis was raised from the nominal value of 1.2 R_e to 2.5 R_e. This was done because all of the reference orbits for Phase II with $r_p = 1.2$ R_e either impacted the Earth, or dipped prohibitively low into the atmosphere. The dramatic lowering of the radius of periapsis is primarily due to the lunar perturbation. *A $1.2R_e$ radius of periapsis for Phase II is not achievable without periodic periapsis raising maneuvers.* It is likely that a higher periapsis will be required for Phase II because with an radius of apogee of 30 R_e, the lunar perturbation lowers periapsis dramatically.

By inspecting the plots in Figure 5 we see that the orbit inclination has the largest influence on the dwell time and maximum eclipse duration. This was also seen for Phase I reference orbits. For Phase II reference orbits we can provide dwell times on the order of 80 days using inclinations around 16°. The maximum eclipse duration for inclinations of 16° varies between 2 and 3 hours depending on Ω and ω. The maximum eclipse duration for these orbits is about 4.5 hours and occurs near inclinations of 23.5°.

Before moving on to discuss the results of the relative motion optimization, it is possible to draw some general conclusions about the reference orbit design. We see that the longest realistic dwell times for Phase I are around 50 days. Dwell times as large as 60 days can be achieved but the orbit inclination must be 10° which is probably prohibitively low. The longest dwell times for phase II are around 85 days and occur at inclinations around 16°. The maximum eclipse duration is intimately dependent on the orbit inclination. Phase I orbits with inclinations higher than 20° experience maximum eclipses of at least 3 hours. Phase II orbits with inclinations higher than 20° experience maximum eclipses in excess of 4 hours. Finally, if a reference orbit is chosen with a period that is an integer number of days, great care must be taken in choosing the epoch of formation establishment. Due to the fact that the plasma sheet has a short period oscillation of one day, reference orbits that have a period that is an integer number of days can yield short dwell times if the initial epoch and the initial true anomaly are not chosen as a coupled pair.

Relative Motion Results

For multiple spacecraft missions such as MMS, designing the relative motion of the spacecraft in formation is in many ways analogous to designing the placement of science instruments on a conventional monolithic single spacecraft platform. Designing the dynamic evolution of the formation

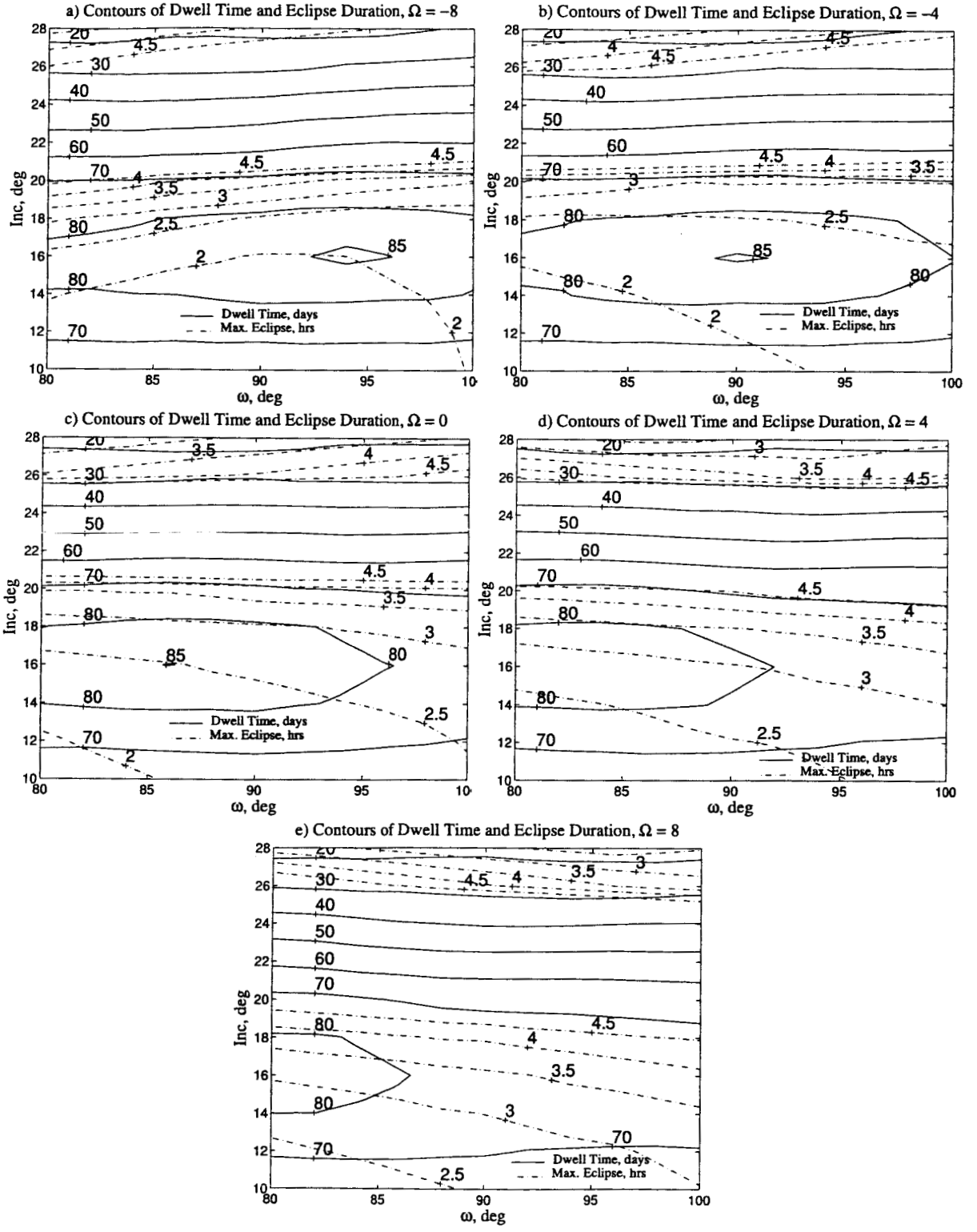

Figure 5: Contours of Dwell Time and Maximum Eclipse Duration for Phase II

is a part of designing the science instrument itself. Here we present some general results for the optimal formation design for MMS and therefore yield insight into the potential performance of MMS as a science instrument. We begin by discussing a single optimal solution for a given region of interest defined by $\nu_i = 160°$ and $\nu_f = 200°$ in Eq. (12). The maximum achievable performance for this solution is presented to illustrate some characteristics of the optimal solutions found in this work. Next we present some general results for the achievable performance over a range of ν_i and ν_c values. We identify the portions of the orbit that can provide useful tetrahedron configurations. Finally, we present results that show how long different formations will remain in optimal configurations in the presence of perturbations.

In Figure 6 we see plots that describe the characteristics of the optimal solution for $\nu_i = 160$ and $\nu_f = 200$ for a Phase I, 10 km tetrahedron. See Table 4 in Appendix 1 for the orbit state information for this solution. The vertical lines in the plots bound the region of interest for the particular solution. The top plot shows the instantaneous performance of the tetrahedron. Recall that the maximum possible performance value at any given instant is three. The two curves in the top plot show the evolution of Q_C and Q_{GM} over one orbit. For a 10 km Phase I tetrahedron Q_C penalizes a solution when the average side length is less than 4 km, and greater than 18 km. Q_C is shown by a solid line. The Glassmeier performance metric, Q_{GM}, is shown by a dotted line. Note both curves were generated using the same orbital states. The only difference in the two curves is the performance metric. The dotted curve gives information about the shape of the formation only. The solid curve gives information about both the size and the shape. The middle plot in Figure 6 shows the lengths of all six sides of the tetrahedron over one complete orbit. The bottom plot shows the average side length over one complete orbit.

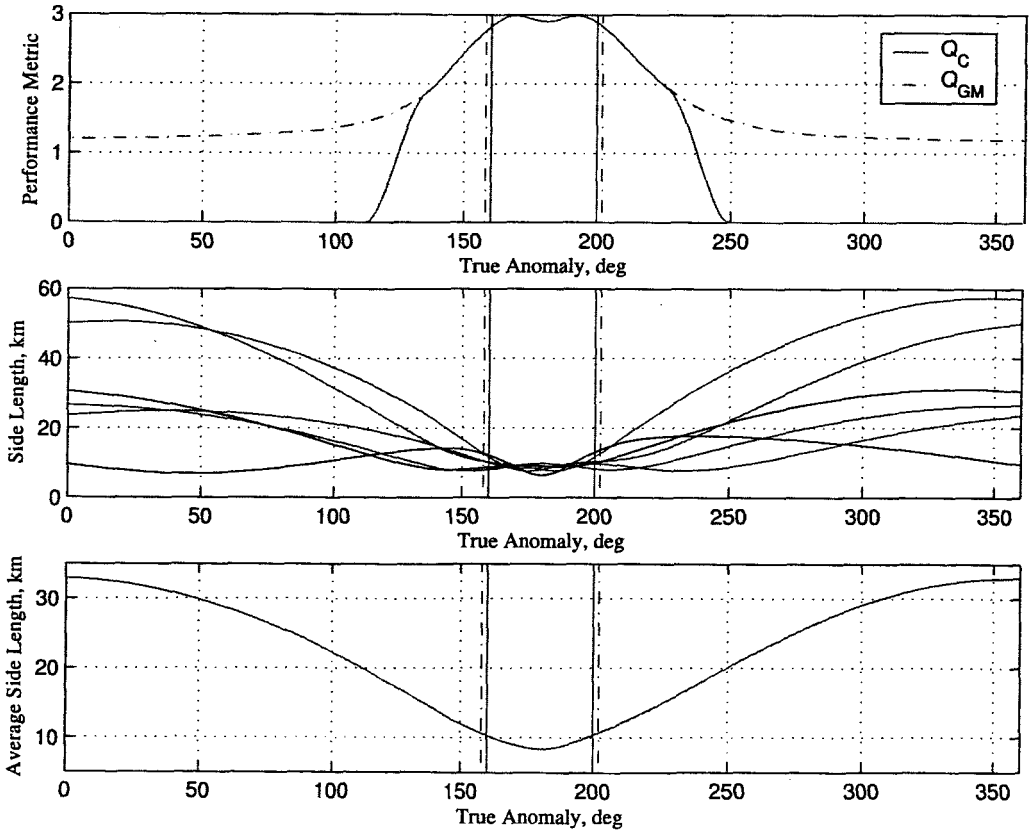

Figure 6: Point Solution One

Examining the top plot in Figure 6, we see that during the region of interest the performance is excellent. The average performance over the region of interest is 2.94. The performance between $\nu_i = 160$ and $\nu_f = 200$ comes at the expense of poor performance outside of the region of interest. From this plot we learn that it is possible to provide excellent performance at orbit apogee for at least +/- 20°. Notice in the second plot in Figure 6 that the side lengths are all near 10 km during the region of interest. Outside the region of interest the side lengths vary between 10 and 60 km. These variations in the side lengths are acceptable according to current design requirements for maximum and minimum inter-spacecraft separations.

While the solution discussed above demonstrates that we can provide excellent performance over significant portions of the orbit, it is not in general possible to provide near ideal performance for the entire orbit. In fact there are regions of the orbit where it is more difficult to maintain regular tetrahedrons. Also, in different portions of the orbit it is possible to maintain regular tetrahedrons for longer periods of time compared to other orbit regions. We need to draw some general conclusions about where in the orbit the best performance can be provided, and for how long.

To aid in generalizing the results of the optimal solutions, we employ a simple change of variables described below

$$\nu_c = (\nu_f + \nu_i)/2 \tag{14}$$

$$\Delta\nu = \nu_f - \nu_i \tag{15}$$

A graphical description of the relationships between ν_c and $\Delta\nu$ and ν_i and ν_f is shown in Figure 7. We have systematically chosen sets of ν_c and $\Delta\nu$ and found optimal solutions to the performance metric shown in Eq. (12) for each pair. We have picked 324 combinations of ν_c and $\Delta\nu$ defined as follows: ν_c is varied from 90° to 270° in increments of 10°. For each value of ν_c we vary $\Delta\nu$ from 10° to 180° in increments of 10°; for each ν_c and $\Delta\nu$ pair an optimal solution has been found for Phase I 10 *km*, Phase I 1000 *km*, and Phase II 10 *km* tetrahedrons.

A contour plot of the optimal average performance vs ν_c and $\Delta\nu$ for 10 km Phase I tetrahedrons is shown in Figure 8. The average performance is defined as the average of the instantaneous performance metric, of the optimized tetrahedron, over the region defined by ν_c and $\Delta\nu$. The plot on the left has $\Delta\nu$ as the independent variable along the y-axis. The plot on the right has the change in time, Δt, that corresponds to the value of $\Delta\nu$ as the independent variable along the y-axis. The two figures allow us to draw some conclusions about the orbit arc length, and the time duration that we can provide acceptable tetrahedron formations. Upon inspection of Figure 8 we see that for regions of $\Delta\nu < 40°$ we can provide average performance levels of 2.95 or better. Recall that the ideal performance according to Eq. (12) is 3.0. We can provide near ideal performance for $\Delta\nu \leq 40°$ within $90° < \nu_c < 270°$.

We see from Figure 8 that the ability to maintain near ideal performance for long trajectory arcs degrades as ν_c moves towards apogee. As an example, for $\nu_c = 180°$ and $\Delta\nu = 100°$ we can provide an average performance of about 2.75. However, for $\nu_c = 90°$ and $\Delta\nu = 100°$ we can provide an average performance of about 2.9. An even more pronounced example occurs at $\nu_c = 90$ and $\Delta\nu = 140°$. In this case we can provide an average performance of 2.8 for a large portion of the orbit. Another general trend in the performance is that it tends to degrade as $\Delta\nu$ increases. For $\Delta\nu = 180°$ we can only provide average performance levels of around 2.65. Due to the fact that the spacecraft velocity is smaller at apogee, it is possible to provide excellent performance for large periods of time for regions near apogee. We assume that average performance values below 2.7 are unacceptable. For average performance levels above 2.7 we assume the formation geometry provides adequate science return. Figure 8 shows that it is possible to achieve acceptable levels of performance for durations near 20 hours for regions centered at apogee. For Phase I, 10 km tetrahedrons, acceptable performance can be maintained for at least 11 hours per orbit, and often much longer, for near-apogee regions.

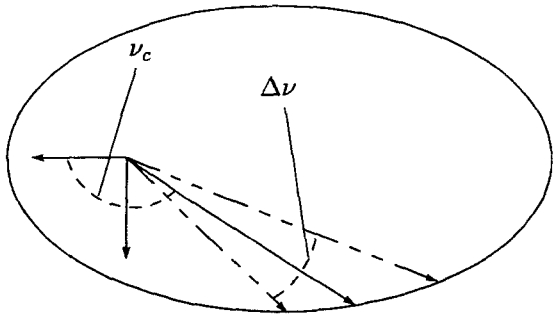

Figure 7: Definition of ν_c and $\Delta\nu$

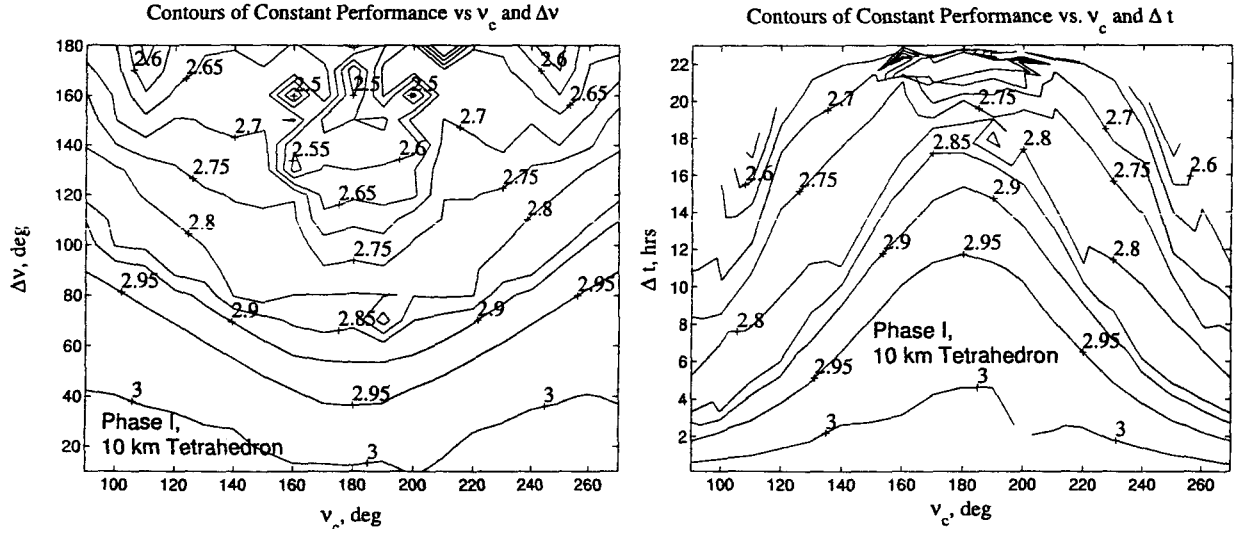

Figure 8: Performance Contours for Phase I, 10 km Tetrahedron

Figure 9 contains plots that illustrate the possible performance for Phase I, 1000 km tetrahedrons. The general relationship between ν_c and $\Delta\nu$ for the Phase I, 1000 *km* performance is similar to the performance curves for the Phase I, 10 *km* tetrahedrons. The ability to maintain near ideal performance for long trajectory arcs degrades as ν_c moves towards apogee. The performance tends to degrade as $\Delta\nu$ increases. For regions of interest centered around apogee, it is still possible to provide an average performance of 2.7 for values of $\Delta\nu$ that are less than 100° and for durations of up to 20 hours per orbit. For off-apogee regions 1000 *km* tetrahedrons that maintain an acceptable average performance can be provided for values of $\Delta\nu$ up to 160° and 9 hours per orbit.

Results for the Phase II, 10 *km* tetrahedron optimization are shown in Figure 10. By comparing the results in Figs. 8-10 we see that changing the dimensions of the reference orbit did not change the general relationship between ν_c, $\Delta\nu$, and the tetrahedron performance. Because the orbit period for Phase II is 3.6 days, we can provide acceptable tetrahedrons during that phase for durations up to 80 hours per orbit. There are some difficulties in designing 1000 *km* tetrahedrons for the nominal Phase II reference orbit. Due to the relatively low altitude of periapsis of 1275 *km* and the large altitude of apoapsis of 185,000 *km*, it is difficult to provide 1000 km tetrahedrons for the current nominal Phase II reference orbit without violating the bound constraints imposed on the

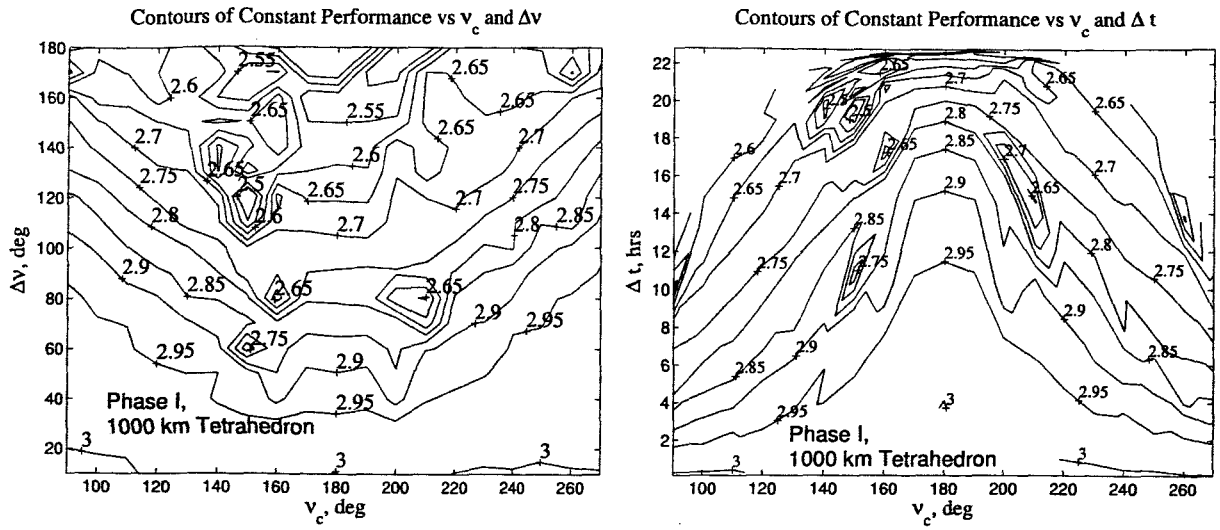

Figure 9: Performance Contours for Phase I, 1000 km Tetrahedron

periapsis altitude shown in Table 3. Due to this reason, and the fact that the current nominal Phase II reference orbit will require frequent periapsis raising maneuvers, data for Phase II 1000 *km* tetrahedrons is not included.

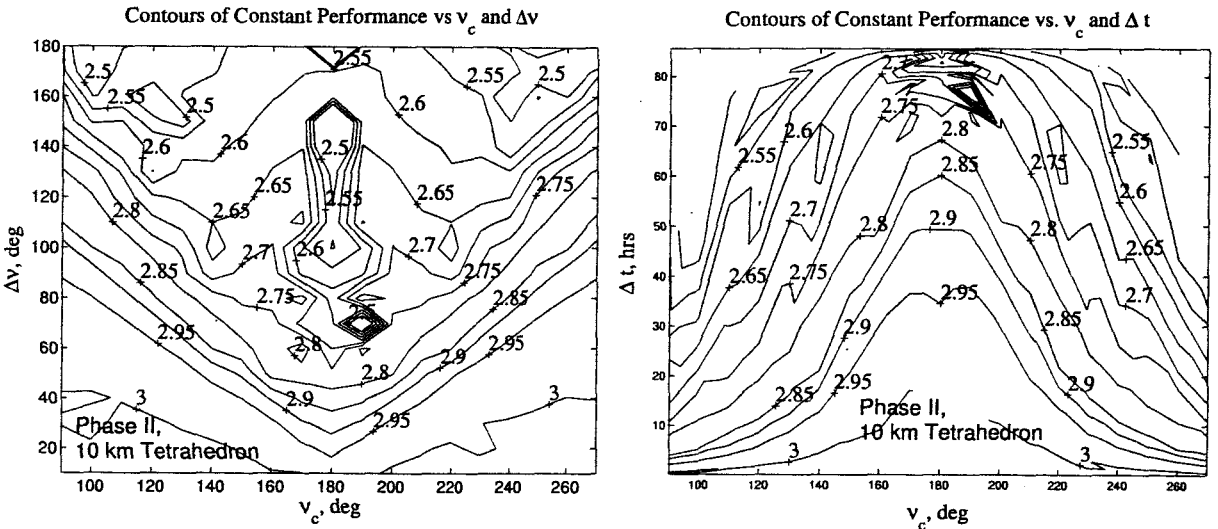

Figure 10: Performance Contours for Phase II, 10 km Tetrahedron

The results above discuss the tetrahedron performance possible under ideal conditions. We neglected to include influences from orbit perturbations and errors in the initial conditions due to navigation uncertainties. We also neglected the close approach constraint outside of the region defined by $\Delta\nu$. However, it is important to determine the stability of the optimal solutions presented above in the presence of perturbations and navigation errors. While a rigorous stability analysis is beyond the scope of this work, we have investigated the evolution of the tetrahedron solutions under the perturbations of the Sun, Moon, and 4x4 non-spherical gravity field. Determining the effects of navigation errors on the orbit performance is a topic of current research. We have taken each solution used to generate the plots in Figures 8-10 and propagated the formations for 50 days under the presence of the perturbations described above. In general, the average performance over

the region defined by ν_c and $\Delta\nu$ decreases with each orbit revolution due to the perturbations. It is assumed that for a particular solution, when the average performance over the region defined ν_c and $\Delta\nu$ drops below 2.7, a maneuver is required to reconfigure the formation.

In Figures 11-13 are plots that contain contours of the time in days for each optimal formation configuration to reach $mean(Q_c) = 2.7$. For both Phase I and II, solutions for $\Delta\nu > 110°$ the formations are highly unstable and only remain in a useful configuration for one day and in some cases less. By comparing the 10 *km* tetrahedron results shown in Figure (11) and (13) we see that for values of ν_c around 180° and values of $\Delta\nu$ around 40° the formations are quite stable and provide acceptable performance for between 30 and 40 days before requiring a maintenance maneuver. Both the 10 *km* and the 1000 *km* tetrahedrons are more stable at off-apogee regions for Phase I.

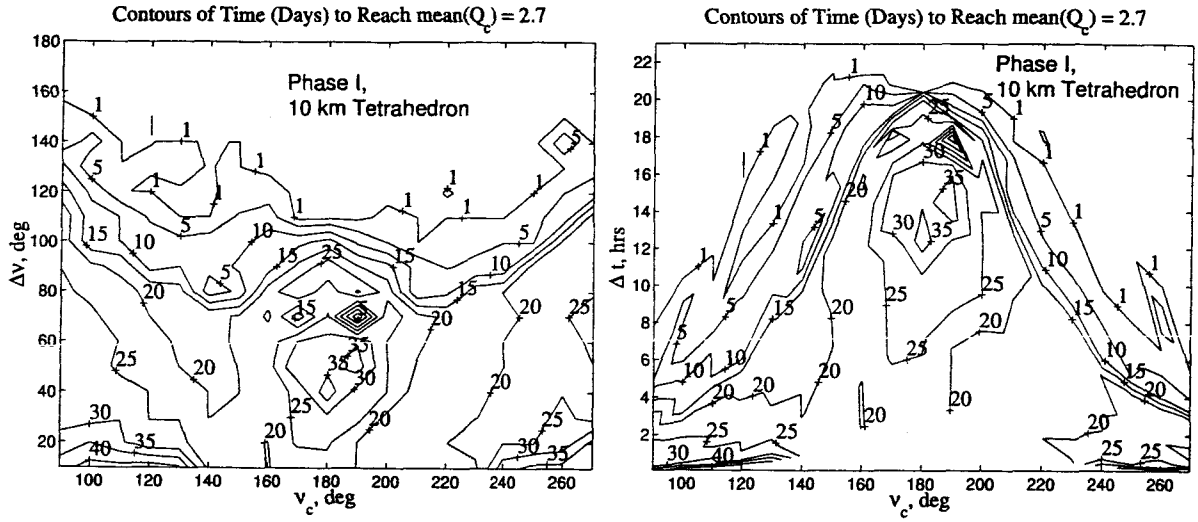

Figure 11: Evolution of Phase I, 10 km Tetrahedron Solutions

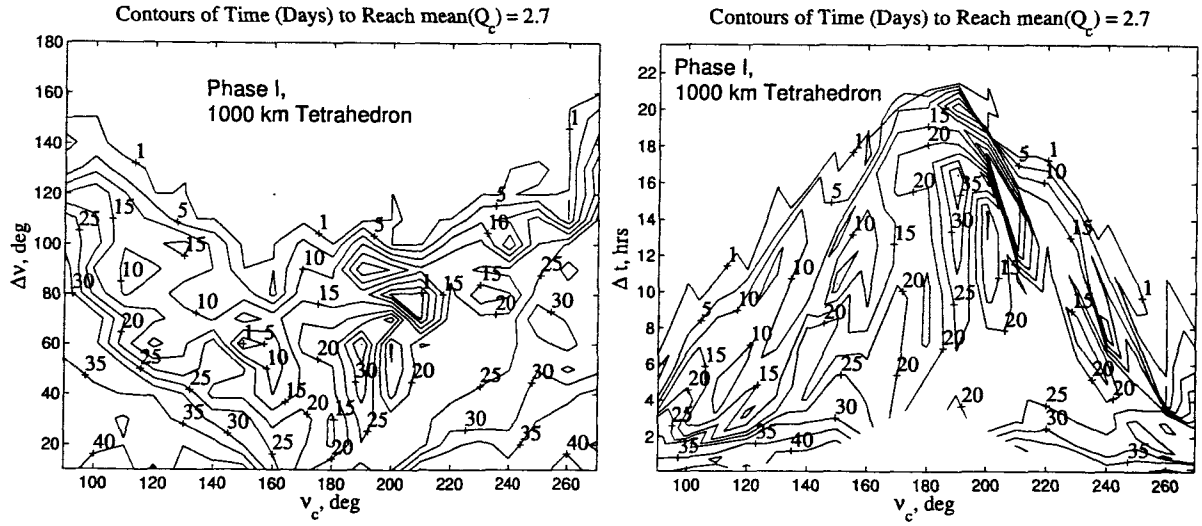

Figure 12: Evolution of Phase I, 1000 km Tetrahedron Solutions

In this section we presented optimal formation solutions for Phase I and II of the MMS mission. The relationship between the reference orbit design and the plasma sheet dwell time and maximum

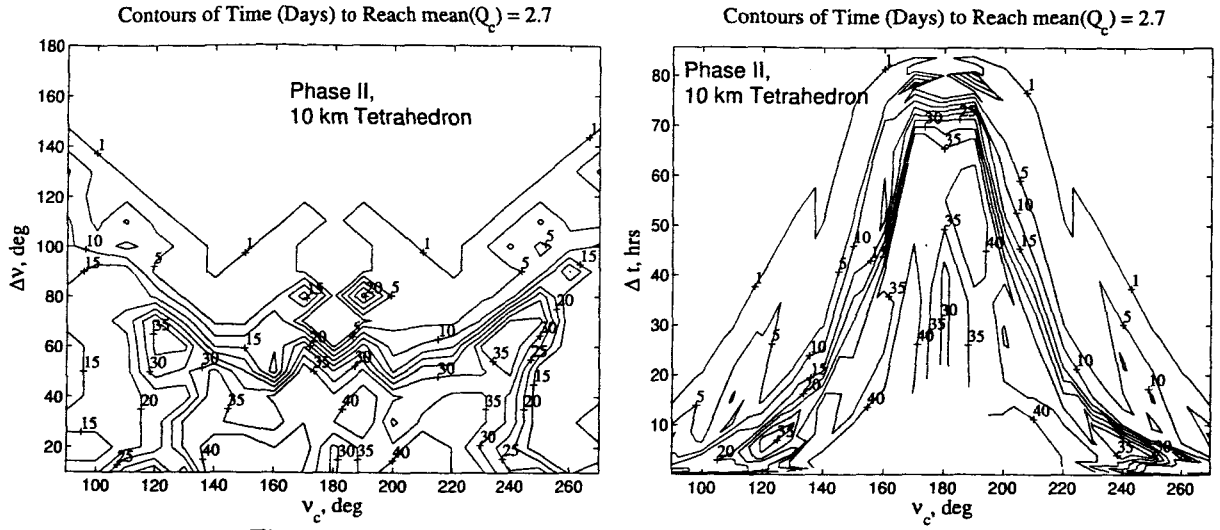

Figure 13: Evolution of Phase II, 10 km Tetrahedron Solutions

eclipse duration was discussed. In general the performance of the tetrahedron, and its stability, varies depending on where in the reference orbit we wish to provide optimal formation configurations.

CONCLUSIONS

For multiple spacecraft missions the coupling between the science return and the orbit design is much stronger than most single spacecraft missions. The stronger coupling is due to the fact that the entire formation serves as the science instrument. The relative geometry of the spacecraft in formation, and the placement of the reference orbit in inertial space, is a part of designing the science instrument itself. The orbit design for MMS plays a large influence on the science return and the resulting scientific advancements made in our understanding of magnetic reconnection, charged particle acceleration, and turbulence in the Earth's magnetosphere.

In this work, we presented optimal orbit designs for Phase I and II of the MMS mission. This entails designing the reference orbits so that the spacecraft dwell-time in the plasma sheet region of the Earth's magnetosphere is a maximum. This is non-trivial because the Earth's magnetosphere is dynamic and its shape and position are not constant in inertial space. Optimal orbit design for MMS also entails designing the formation so that the relative motion of the four spacecraft is optimal according to a metric directly related to the science performance. We developed a performance metric that is related to the science return, and use Sequential Quadratic Programming (SQP) to determine optimal relative motion solutions for different regions of interest along the reference orbit.

We found that the longest realistic dwell time for the nominal Phase I orbit is around 50 days. This is dependent on the current dimensions of the nominal orbit which are determined by the science goals. Different maximum dwell times will result for different reference orbit dimensions. Dwell times as large as 60 days can be achieved for the nominal Phase I orbit but the orbit inclination must be 10° which is most likely prohibitively low. The longest dwell times for phase II are around 85 days and occur at inclinations around 16°. The maximum eclipse duration is intimately dependent on the orbit inclination. Phase I orbits with inclinations higher than 20° experience maximum eclipses of at least 3 hours. Phase II orbits with inclinations higher than 20° experience maximum eclipses in excess of 4 hours. The current nominal Phase II reference orbit will require maneuvers to ensure that the orbit does not reenter or dip prohibitively low into the Earth's atmosphere. Finally, if a

reference orbit is chosen with a period that is an integer number of days, great care must be taken in choosing the epoch of formation establishment. Due to the fact that the plasma sheet has a short period oscillation of one day, reference orbits that have a period that is an integer number of days can yield short dwell times if the initial epoch and the initial true anomaly are not chosen as a coupled pair.

The relative motion of the MMS formation must provide an appropriate tetrahedron shape, as well as size. We used a metric previously presented in Refs. [2] and [3] to design optimal relative motion solutions for different regions in the reference orbit. In general, for Phase I, it is possible to achieve acceptable levels of performance for durations near 20 hours per orbit for regions centered at apogee. For Phase I, 10 km tetrahedrons, acceptable performance can be maintained for at least 11 hours per orbit, and often much longer, for off-apogee regions. For Phase II we can provide acceptable tetrahedrons for durations up to 80 hours per orbit. A preliminary analysis was performed to determine how the optimal tetrahedrons evolve under the influence of orbit perturbations. Neglecting navigation uncertainties, and some possible close approaches, some solutions remain in acceptable configurations for up to 40 days.

REFERENCES

[1] S. Curtis, "The Magnetospheric Multiscale Mission...Resolving Fundamental Processes in Space Plasmas," *NASA Technical Memorandum*, NASA/GSFC, 2000.

[2] S. Hughes, "Formation Tetrahedron Design for Phase I of the Magnetospheric Multiscale Mission", Proceedings of the 2004 Flight Mechanics Symposium, NASA Goddard Space Flight Center, Oct. 2003.

[3] G. Paschmann and P. W. Daly, "Analysis Methods for Multi-Spacecraft Data", ESA Publications Division, Netherlands, 1998.

[4] D.A. Vallado, "Fundamentals of Astrodynamics and Applications, 2nd Edition", Kluwer Academic Publishers, Dordrecht, 2001.

[5] *Optimization Toolbox User's Guide.* The Mathworks,

[6] D.P. Stern, "Systematic Indentification of Preferred Orbits for Magnetosperic Mission: 1. Single Satellites", Journal of the Astronautical Sciences, Nov.-Dec. 2001.

[7] D.P. Stern, "Systematic Indentification of Preferred Orbits for Magnetosperic Mission: 2. The "Profile" Constellation", Journal of the Astronautical Sciences, Vol. 50, No. 2, 2001.

[8] N. A. "Tsyganenko, A Magnetospheric Magnetic Field Model with a Warped Tail Current Sheet", Planet. Space Sci. Vol. 37, 1989.

[9] N. A. "Tsyganenko, Modeling the Earth's Magnetospheric Magnetic Field Confined Within a Realistic Magnetopause", J.Geophys.Res., Vol. 100, 1995.

[10] N. A. "Tsyganenko and D.P. Stern, Modeling the Global Magnetic Field of the Large-Scale Birkeland Current Systems", J. Geophys.Res., Vol. 101, 1996.

[11] N. A. "Tsyganenko, A model of the near magnetosphere with a dawn-dusk asymmetry - 1. Mathematical Structure", J. Geophys.Res., Vol. 107, 2002.

[12] N. A. "Tsyganenko, A model of the near magnetosphere with a dawn-dusk asymmetry - 2. Parameterization and fitting to observations", J. Geophys.Res., Vol. 107,2002.

APPENDIX

Table 4: States Associated with Figure 6

State Variable	Orbit One	Orbit Two	Orbit Three	Orbit Four
a (km)	42256.691	42256.691	42256.691	42256.691
e	0.80229	0.80221	0.80214	0.80220
i (deg.)	10.0481	10.0493	10.0486	10.0426
ω (deg.)	90.2462	90.2623	90.2540	90.2591
Ω (deg.)	-0.06204	-0.06873	-0.07096	-0.07084
ν (deg.)	180.1627	180.1585	180.1634	180.1608